Shakedown analysis of a torispherical head with a piping nozzle under combined loads by the stress compensation method

Heng Peng[1], Jun Shen[1], Yinghua Liu[1,*], Haofeng Chen[2]

[1]*Department of Engineering Mechanics, AML, Tsinghua University, Beijing 100084, People's Republic of China*

[2]*Department of Mechanical and Aerospace Engineering, University of Strathclyde, Glasgow G1 1XJ, UK*

E-mail address: pengheng17@mails.tsinghua.edu.cn (Heng Peng), kennyshen@vip.163.com (Jun Shen), yhliu@mail.tsinghua.edu.cn (Yinghua Liu), haofeng.chen@strath.ac.uk (Haofeng Chen)

ABSTRACT: Shakedown assessment is an important task in determining the load-bearing capacity of structures and evaluating their safety. The traditional shakedown analyses, which are based on the upper or lower bound shakedown theorem to establish the mathematical programming formulation and solve an optimisation problem, are difficult to apply in engineering practice owing to limitations of the computing scale and computational efficiency. In this study, a numerical shakedown analysis using the recently developed stress compensation method (SCM) is performed for a torispherical head with a piping nozzle, which is a typical structural component of pressure vessel equipment. The loads applied to the structural component include an internal pressure, axial force, twisting moment, out-of-plane and in-plane bending moments, and thermal loading, all of which vary independently of each other. Two- and three-dimensional strict shakedown boundaries for the torispherical head under different combinations of these loads are presented and analysed. In addition, the effect of a temperature-dependent yield strength on the shakedown domain is also investigated. These investigations demonstrate that the proposed SCM is capable of solving the practical shakedown problem for structures under complicated combined loads in industrial applications. The obtained results can provide guidance for the safe structural design of torispherical heads with piping nozzles.

Keywords: shakedown; torispherical head; nozzle; temperature-dependent yield strength; stress compensation method

[*]Corresponding author

E-mail address: yhliu@mail.tsinghua.edu.cn (Yinghua Liu)

Nomenclature

$\boldsymbol{x}$	Coordinate vector of a material point	$\dot{\boldsymbol{u}}(t)$, $\Delta\boldsymbol{u}$	Nodal displacement rate, nodal displacement increment
t, t_i	Time, time point (or load vertex *i*)	$\boldsymbol{\sigma}^C(t)$	Compensation stress vector
$\boldsymbol{\sigma}(\boldsymbol{x},t)$, $\boldsymbol{\sigma}(t)$	Total stress vector	$\bar{\sigma}(t)$	von Mises equivalent stress
$\boldsymbol{\sigma}^E(\boldsymbol{x},t)$, $\Delta\boldsymbol{\sigma}^E$, $\dot{\boldsymbol{\sigma}}^E(t)$	Fictitious elastic stress vector, its increment, its rate	$\boldsymbol{K}$	Structural global stiffness matrix
$\boldsymbol{\rho}(\boldsymbol{x},t)$, $\Delta\boldsymbol{\rho}$, $\dot{\boldsymbol{\rho}}(t)$, $\boldsymbol{\rho}_0^{(m+1)}$, $\boldsymbol{\rho}_0^{(m)}$	Residual stress vector, its increment, its rate, new residual stress vector for shakedown , old residual stress vector for shakedown	$\sigma_y(\theta)$, σ_{y_0}	Yield strength depending on temperature θ, yield strength at 20 °C
NV	Number of load vertices	D_a	Outer diameter of the cylindrical vessel
$\boldsymbol{P}_i(\boldsymbol{x},t)$	*i*th load vector	t_e	Thickness of the cylindrical vessel
$\mu_i(t)$, μ_i^-, μ_i^+	Time-dependent factor of *i*th loading, its lower bound, its upper bound	r	Radius of the knuckle
$\boldsymbol{P}_i^0(\boldsymbol{x})$	Base load vector of *i*th loading	R	Radius of the head crown
$\boldsymbol{P}(\boldsymbol{x},t)$	Total load vector	t_s	Thickness of the nozzle
$\boldsymbol{\sigma}_i^0(\boldsymbol{x})$	Fictitious elastic stress vector of a body under $\boldsymbol{P}_i^0(\boldsymbol{x})$	d_i	Inner diameter of the nozzle
$\boldsymbol{\sigma}_i(\boldsymbol{x},t)$	Fictitious elastic stress vector of a body under $\boldsymbol{P}(\boldsymbol{x},t)$	c_a	Offset of the nozzle
λ	Load multiplier	P, P_0	Internal pressure, its fundamental load
f	Yield function	F, F_0	Axial force, its fundamental load
θ	Temperature	T, T_0	Twisting moment, its fundamental load
$\nabla\cdot$	Divergence operator	M_{out}, $M_{\text{out}0}$	Out-of-plane bending moment, its fundamental load
$\boldsymbol{n}$	Unit outward normal	M_{in}, $M_{\text{in}0}$	In-plane bending moment, its fundamental load
$\dot{\boldsymbol{\varepsilon}}(t)$	Total strain rate	$\Delta\theta$, $\Delta\theta_0$	Temperature difference, its fundamental load
$\dot{\boldsymbol{\varepsilon}}^E(t)$	Fictitious elastic strain rate	E	Young's modulus
$\dot{\boldsymbol{\varepsilon}}_\theta(t)$, $\Delta\boldsymbol{\varepsilon}_\theta(t_i)$	Thermal strain rate, thermal strain increment	v	Poisson's ratio
$\dot{\boldsymbol{\varepsilon}}^p(t)$	Plastic strain rate	α	Coefficient of thermal expansion
$\dot{\boldsymbol{\varepsilon}}_r^e(t)$	Residual elastic strain rate	c	Specific heat capacity
$\boldsymbol{D}$	Elastic coefficient matrix	k	Thermal conductivity
$\boldsymbol{B}$	Strain-displacement matrix	ρ	Density

1. Introduction

During the structural design and integrity assessment of pressure vessels and pipelines, it is very important to predict the long-term behaviour and load-bearing capacity of their structural components accurately. Owing to the startup, shutdown, and load fluctuation of these equipment, they are usually subjected to variable repeated loads during their service life. If the applied load is much higher than the design value, the structural components may experience instantaneous plastic collapse. Often, the structure may fail after some working time through two mechanisms: one is incremental plasticity (or ratcheting), in which the structure bulges and plastic deformation accumulates continually with increasing of load cycles; the other is alternating plasticity (or low cycle fatigue), in which plastic strains appear alternately, but their sum is equal to zero over a load cycle. If the applied load is lower than a certain value, the plastic deformation will vary through some number of initial load cycles, after which the structure will respond with elastic behaviour. This stabilisation of the plastic deformation is called a strict shakedown (or elastic shakedown) and allows the structure to maintain a long-term safety status. Therefore, many engineering design specifications, such as the ASME Code, R5 and R6 procedures, RCC-MR standard, and European pressure vessel EN 13445-3 standard, include a shakedown assessment as one of the criteria for a structural design and safety evaluation.

In addition to the simplified assessment criteria given in the relevant standards, there are two further methods used to determine the shakedown limit: step-by-step incremental analysis and the direct method [1-4]. As a general approach, the former method first predicts the cyclic behaviour of structures under a given loading history, and then adjusts the applied load to approach to the shakedown limit via a series of trial-and-error procedures [3]. However, the calculation process for this method is very complicated and the computational cost is excessive, especially when large-scale structures under multiple variable loads are considered. As a better alternative, the direct method can calculate the shakedown limit load directly and efficiently. In general, the shakedown analysis in this method is based on the lower or upper shakedown theorem [1, 2], through which the shakedown problem is transformed into the solution of an extreme function with a large number of equality and inequality constraints. Different optimisation methods such second-order cone programming [5], the complex method [6], interior point method (IPM) [7-9], and Newton-like iteration method [10-13] are utilised to solve the mathematical programming problem. Some applications of these methods for engineering structures have been reported in literature [13-15]. There are also some other shakedown analysis methods with more physical arguments, such as the m(alpha)-method [16], elastic compensation method [17, 18], non-cyclic shakedown method [19-21], residual stress decomposition method [22], linear matching method (LMM) [23, 24], and stress

compensation method (SCM) [25]. Among these numerical methods, LMM and SCM have been implemented in commercially available finite element software and proven to be suitable for solving practical complex engineering problems.

A cylindrical pressure vessel with torispherical heads is a typical equipment component in the petroleum and chemical industries. Owing to the requirements of its producing function, pressure vessels are often manufactured with a piping nozzle attached to the torispherical head. Some nozzles are placed in the knuckle region. The presence of these piping nozzles weakens the load-bearing capacity of the pressure vessel. On one hand, the stress level in the knuckle region of the torispherical head with nozzles is increased due to stress concentration. On the other hand, additional forces are generated between the nozzle and torispherical head due to their mutual restraint when the temperature and load change. However, in practical engineering design, it is difficult to consider these loading conditions fully and to investigate the effects of random variation in these loads on the load-bearing capacity of the structure. Therefore, it is necessary to determine the strict shakedown limit or shakedown domain of the torispherical head with a piping nozzle under some possible loading scenario.

Assessment of the shakedown limit and plastic collapse load of such structures is attractive to many researchers and has been incorporated in some design codes [15]. Saal et al. [26] investigated the flexibility factors for nozzles in the knuckle region of a torispherical head to enable the restraint moments and forces acting on the nozzles to be properly considered in the design. Hsieh et al. [27, 28] calculated the elastic limits and plastic collapse loads of structures subjected to combined pressure and piping loads. Considering the cyclic load, some two- and three-dimensional shakedown domains of the heads were determined by Tran et al. [15] and Simon et al. [14]. However, in these studies, only parts of the loading conditions are considered, and shakedown analyses with a temperature-dependent yield strength have not been reported.

In this study, the recently proposed SCM is utilised to investigate the shakedown domains of a torispherical head with a piping nozzle under an internal pressure, axial force, twisting moment, out-of-plane and in-plane bending moments, and thermal loading. More comprehensive loading conditions and more sophisticated finite element models are considered, and the effect of the temperature-dependent yield strength on the shakedown domain of the structure is also analysed. The remainder of this paper is outlined as follows: Section 2 describes the procedure for the shakedown analysis based on the SCM. Next, the model and some elastic stress calculations are presented, and verification of the shakedown and limit analyses of the structure under a single load are performed in Section 3 using the elastic-plastic incremental method in the Abaqus finite element software [29]. Then, the shakedown domains of the torispherical head with a piping nozzle under different combined loads are presented and discussed in Section 4. Finally, conclusions from the results of these

numerical investigations are drawn in Section 5.

2. SCM for shakedown analysis

2.1. Melan's static shakedown theorem

Considering a structural body, V, subjected to thermomechanical loading. If plastic deformation occurs in the body, the total stress, $\boldsymbol{\sigma}(\boldsymbol{x},t)$, of a material point, $\boldsymbol{x}$, can be decomposed into the fictitious elastic stress, $\boldsymbol{\sigma}^E(\boldsymbol{x},t)$, and the residual stress, $\boldsymbol{\rho}(\boldsymbol{x},t)$, as follows:

$$\boldsymbol{\sigma}(\boldsymbol{x},t)=\boldsymbol{\sigma}^E(\boldsymbol{x},t)+\boldsymbol{\rho}(\boldsymbol{x},t) \tag{2}$$

where $\boldsymbol{\sigma}^E(\boldsymbol{x},t)$ is the stress solution of the fictitious elastic reference body, V^E, under the same load conditions. The structural body, V, may be subjected to multiple loading cases, $\boldsymbol{P}_i(\boldsymbol{x},t), i=1,2,\cdots,N$, where each loading case, $\boldsymbol{P}_i(\boldsymbol{x},t)$, is represented as the product of a time-dependent factor, $\mu_i(t)$, and a base load, $\boldsymbol{P}_i^0(\boldsymbol{x})$. Thus, the loading history, $\boldsymbol{P}(\boldsymbol{x},t)$, is expressed as combinations of these N loading cases:

$$\boldsymbol{P}(\boldsymbol{x},t)=\sum_{i=1}^{N}\boldsymbol{P}_i(\boldsymbol{x},t)=\sum_{i=1}^{N}\mu_i(t)\boldsymbol{P}_i^0(\boldsymbol{x}) \tag{3}$$

Referring to Eq. (3), the fictitious elastic stress, $\boldsymbol{\sigma}^E(\boldsymbol{x},t)$, can also be decomposed according to the loading cases as follows:

$$\boldsymbol{\sigma}^E(\boldsymbol{x},t)=\sum_{i=1}^{N}\boldsymbol{\sigma}_i(\boldsymbol{x},t)=\sum_{i=1}^{N}\mu_i(t)\boldsymbol{\sigma}_i^0(\boldsymbol{x}) \tag{4}$$

where the base stress, $\boldsymbol{\sigma}_i^0(\boldsymbol{x})$, is calculated through an elastic finite element analysis of the body under the base load, $\boldsymbol{P}_i^0(\boldsymbol{x})$; $\boldsymbol{\sigma}_i(\boldsymbol{x},t)$ is the corresponding stress case.

The static shakedown theorem for a structural body composed of materials with a temperature-dependent yield strength is stated as follows: the structural body will shake down if there exists a time-independent self-equilibrated residual stress field, $\boldsymbol{\rho}(\boldsymbol{x})$, such that its superposition with the fictitious elastic stress field, $\lambda\cdot\boldsymbol{\sigma}^E(\boldsymbol{x},t)$, results in a safe stress state, $\boldsymbol{\sigma}(\boldsymbol{x},t)$, at every point of the body, i.e. the structural body responds elastically after several loading cycles [30].

$$\boldsymbol{\sigma}(\boldsymbol{x},t)=\lambda\cdot\boldsymbol{\sigma}^E(\boldsymbol{x},t)+\boldsymbol{\rho}(\boldsymbol{x}) \tag{5}$$

$$\begin{aligned} &f=F\left(\boldsymbol{\sigma}(\boldsymbol{x},t)\right)-\sigma_y(\theta)\le 0 \qquad \forall\boldsymbol{x}\in V,\ \forall t\\ &\nabla\cdot\boldsymbol{\rho}(\boldsymbol{x})=0 \qquad \text{in } V\\ &\boldsymbol{\rho}(\boldsymbol{x})\cdot\boldsymbol{n}=0 \qquad \text{on } S_t \end{aligned} \tag{6}$$

where λ is the load multiplier; f is the yield function; $\sigma_y(\theta)$ is the yield strength, which is dependent on the temperature, θ; $\nabla\cdot$ is the divergence operator; and $\boldsymbol{n}$ is the unit outward normal to the surface, S_t.

It is worth noting that in practical situations the loading histories, $\mu_i(t)$, are usually unknown but their bounds are known. If the bounds of each loading case are assumed as follows:

$$\mu_i^- \le \mu_i(t) \le \mu_i^+ \tag{7}$$

the bounding envelope of the loading history can also be determined. Then, all of the possible loading histories within this bounding envelope define a loading domain, $\boldsymbol{\Omega}$, which is often a polyhedron containing $NV = 2^N$ vertices. As an example, considering three loads that vary independently of each other within their own limits, the loading history, $\boldsymbol{P}(\boldsymbol{x},t)$, must be within a loading domain with eight vertices (i.e. B^1, B^2, B^3, B^4, B^5, B^6, B^7 and B^8) in the three-dimensional loading space, as shown in Fig. 1.

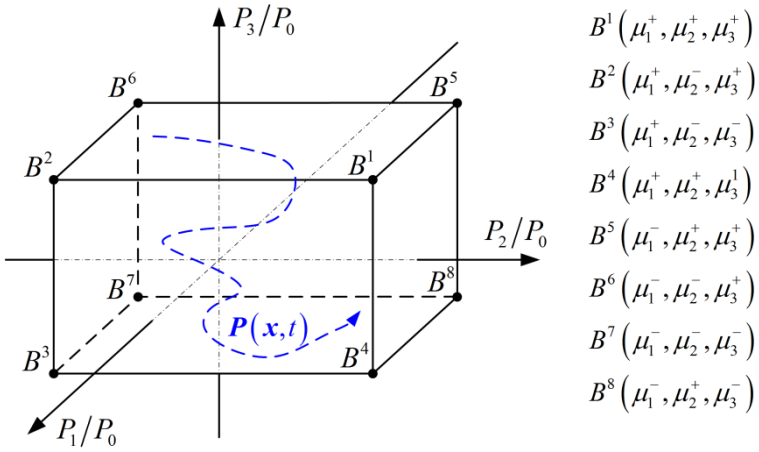

Fig. 1. A loading domain with eight vertices in the three-dimensional loading space.

According to the theorem proposed by König [3], the shakedown boundary for a structure subjected to three loads varying independently can be determined by estimating the shakedown limit of the structure under a specific loading history that traverses the eight vertices of the brick loading domain. A more detailed explanation of this process are available in Reference [25].

2.2. SCM

The SCM has been detailed in previous studies [25]. For convenience, a basic overview is presented here. The key idea of a static shakedown analysis is to search for the optimal residual stress field.

The total strain rate, $\dot{\boldsymbol{\varepsilon}}(t)$, includes the elastic strain rate, $\dot{\boldsymbol{\varepsilon}}^E(t)$, thermal strain rate, $\dot{\boldsymbol{\varepsilon}}_\theta(t)$, plastic strain rate, $\dot{\boldsymbol{\varepsilon}}^p(t)$, and residual elastic strain rate, $\dot{\boldsymbol{\varepsilon}}_r^e(t)$, as follows:

$$\dot{\boldsymbol{\varepsilon}}(t)=\lambda\left[\dot{\boldsymbol{\varepsilon}}^{E}(t)+\dot{\boldsymbol{\varepsilon}}_{\theta}(t)\right]+\dot{\boldsymbol{\varepsilon}}^{p}(t)+\dot{\boldsymbol{\varepsilon}}_{r}^{e}(t) \tag{8}$$

The finite element global equilibrium equations can then be established as the following:

$$\left(\int_{V}\boldsymbol{B}^{T}\cdot\boldsymbol{D}\cdot\boldsymbol{B}dV\right)\cdot\dot{\boldsymbol{u}}(t)=\lambda\int_{V}\boldsymbol{B}^{T}\cdot\boldsymbol{D}\cdot\left[\dot{\boldsymbol{\varepsilon}}^{E}(t)+\dot{\boldsymbol{\varepsilon}}_{\theta}(t)\right]dV+\int_{V}\boldsymbol{B}^{T}\cdot\boldsymbol{D}\cdot\dot{\boldsymbol{\varepsilon}}^{p}(t)dV \tag{9}$$

The term $\boldsymbol{D}\cdot\dot{\boldsymbol{\varepsilon}}^{p}(t)$ is replaced by the compensation stress, $\boldsymbol{\sigma}^{C}(t)$, which is calculated with the following:

$$\boldsymbol{\sigma}^{C}(t)=\xi(t)\cdot\boldsymbol{\sigma}(t),\quad \xi(t)=\begin{cases}\dfrac{\bar{\sigma}(t)-\sigma_{y}(\theta)}{\bar{\sigma}(t)} & \left(\bar{\sigma}(t)>\sigma_{y}(\theta)\right)\\ 0 & \left(\bar{\sigma}(t)\le\sigma_{y}(\theta)\right)\end{cases} \tag{10}$$

where $\bar{\sigma}(t)$ is the von Mises equivalent stress of the stress state, $\boldsymbol{\sigma}(t)$, Eq. (9) can then be written as follows:

$$\boldsymbol{K}\cdot\dot{\boldsymbol{u}}(t)=\lambda\int_{V}\boldsymbol{B}^{T}\cdot\dot{\boldsymbol{\sigma}}^{E}(t)dV+\lambda\int_{V}\boldsymbol{B}^{T}\cdot\boldsymbol{D}\cdot\dot{\boldsymbol{\varepsilon}}_{\theta}(t)dV+\int_{V}\boldsymbol{B}^{T}\cdot\boldsymbol{\sigma}^{C}(t)dV \tag{11}$$

where $\boldsymbol{K}=\int_{V}\boldsymbol{B}^{T}\cdot\boldsymbol{D}\cdot\boldsymbol{B}dV$ is the structural global stiffness matrix. The residual stress field for the shakedown analysis can be calculated with the following:

$$\dot{\boldsymbol{\rho}}(t)=\boldsymbol{D}\cdot\boldsymbol{B}\cdot\dot{\boldsymbol{u}}(t)-\lambda\dot{\boldsymbol{\sigma}}^{E}(t)-\lambda\boldsymbol{D}\cdot\dot{\boldsymbol{\varepsilon}}_{\theta}(t)-\boldsymbol{\sigma}^{C}(t) \tag{12}$$

$$\boldsymbol{\rho}(t+\Delta t)=\boldsymbol{\rho}(t)+\int_{t}^{t+\Delta t}\dot{\boldsymbol{\rho}}(t)dt \tag{13}$$

For each load vertex *i* (or time point, t_i), the total stress at every Gauss point of a body is determined as follows:

$$\boldsymbol{\sigma}(t_i)=\lambda\boldsymbol{\sigma}^{E}(t_i)+\boldsymbol{\rho}(t_i) \tag{14}$$

The compensation stress, $\boldsymbol{\sigma}^{C}(t_i)$, is calculated using Eq. (10). Considering that Eq. (11) is solved for *NV* load vertices, the *NV* expressions of Eqs. (11) and (12) are superposed over a load cycle, yielding the following expressions:

$$\boldsymbol{K}\cdot\Delta\boldsymbol{u}=\sum_{i=1}^{NV}\left\{\lambda\int_{V}\boldsymbol{B}^{T}\cdot\left[\Delta\boldsymbol{\sigma}^{E}(t_i)+\boldsymbol{D}\cdot\Delta\boldsymbol{\varepsilon}_{\theta}(t_i)\right]dV+\int_{V}\boldsymbol{B}^{T}\cdot\boldsymbol{\sigma}^{C}(t_i)dV\right\} \tag{15}$$

$$\Delta\boldsymbol{\rho}=\boldsymbol{D}\cdot\boldsymbol{B}\cdot\Delta\boldsymbol{u}-\lambda\sum_{i=1}^{NV}\Delta\boldsymbol{\sigma}^{E}(t_i)-\lambda\boldsymbol{D}\cdot\sum_{i=1}^{NV}\Delta\boldsymbol{\varepsilon}_{\theta}(t_i)-\sum_{i=1}^{NV}\boldsymbol{\sigma}^{C}(t_i) \tag{16}$$

For the inner iteration, *m*, the residual stress, $\boldsymbol{\rho}_{0}^{(m+1)}$, for shakedown can be updated as follows:

$$\boldsymbol{\rho}_{0}^{(m+1)}=\boldsymbol{\rho}_{0}^{(m)}+\Delta\boldsymbol{\rho}_{0}^{(m+1)},\quad \text{where}\quad \Delta\boldsymbol{\rho}_{0}^{(m+1)}=\frac{1}{NV}\Delta\boldsymbol{\rho}^{(m+1)} \tag{17}$$

where $\boldsymbol{\rho}_{0}^{(m+1)}$ is the new residual stress, $\boldsymbol{\rho}_{0}^{(m)}$ is the old residual stress, and $\Delta\boldsymbol{\rho}_{0}^{(m+1)}$ is the residual stress increment. Using the same iteration control technique as that in [25], the numerical procedure of the SCM for shakedown analysis considering the temperature-dependent yield strength is shown in Fig. 2.

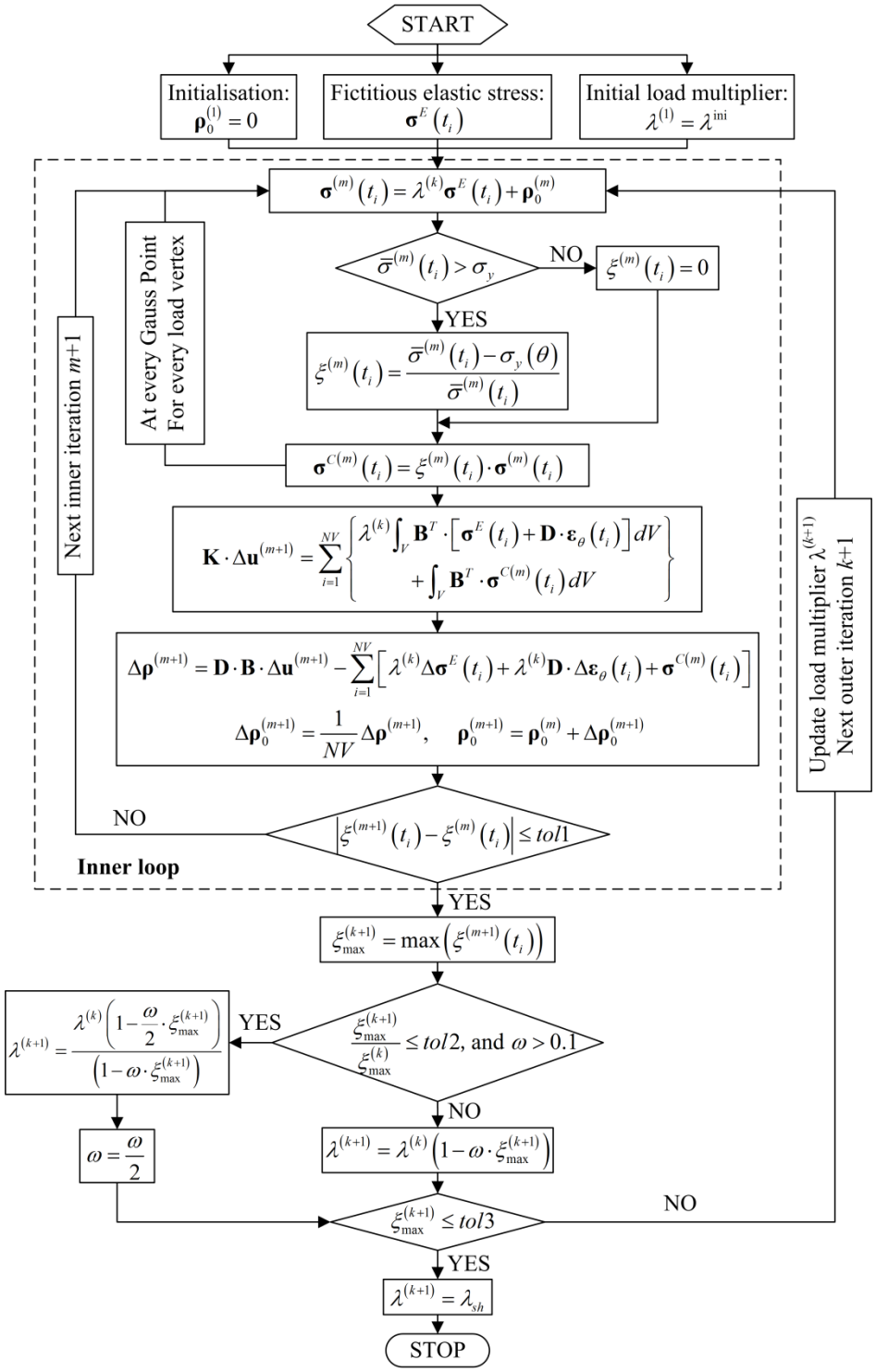

158

159 **Fig. 2.** Flowchart of the SCM for shakedown analysis.

160 ## 3. Model and validation

161 ### 3.1. Geometry and material

162 Fig. **3** shows the geometry of the Klöpperböden torispherical head with a piping nozzle, which has been
163 studied previously by several authors [14, 15, 26, 27]. The outer diameter and thickness of the cylindrical vessel

are D_a and t_e, respectively. The radii of the knuckle and the head crown are r and R, respectively. The inner diameter and thickness of the nozzle are d_i and t_s, respectively. The axial line of the nozzle is parallel to the axial line of the cylindrical vessel, and the distance of the farthest point on the middle surface of the nozzle shell from the axial line of the cylindrical vessel is c_a. Detailed dimensions of the torispherical head with a piping nozzle are listed in Table 1. A uniform pressure, P, acts on the inside surfaces of the cylindrical vessel and the nozzle. An axial force, F, twisting moment, T, out-of-plane bending moment, M_{out}, and in-plane bending moment, M_{in}, are applied to the end of the nozzle. In addition, thermal loading is applied by defining a temperature difference, $\Delta\theta$, between the inside and outside surfaces of the cylindrical vessel and the nozzle. The structure is constructed of an elastic-perfectly plastic material, and its basic material properties are listed in Table 2.

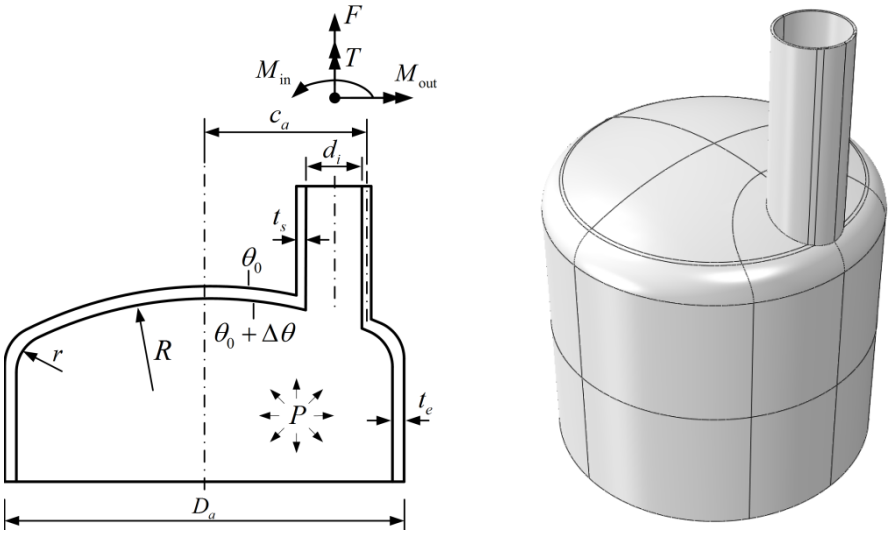

Fig. 3. Geometry of the torispherical head with a piping nozzle.

Table 1 Dimensions of the torispherical head with a piping nozzle [mm].

Outer diameter of the cylindrical vessel, D_a	2000
Thickness of the cylindrical vessel, t_e	14
Radius of the knuckle, r	200
Radius of the head crown, R	2000
Thickness of the nozzle, t_s	13.6
Inner diameter of the nozzle, d_i	400
Offset of the nozzle, c_a	910

Table 2 Material properties of the torispherical head with a piping nozzle.

Yield strength, σ_{y_0} [MPa]	340
Young's modulus, E [MPa]	2.0×10^5
Poisson's ratio, v	0.3
Coefficient of thermal expansion, α [/°C]	1.6×10^{-5}
Specific heat capacity, c [J/(kg·°C)]	500
Thermal conductivity, k [W/(m·°C)]	15
Density, ρ [kg/m^3]	7900

3.2. Finite element model and elastic stress calculation

3.2.1. Finite element model

Although the geometry of the torispherical head with a piping nozzle is symmetrical, its loading condition does not meet the requirements for a symmetric model owing to the existence of the out-plane bending moment and twisting moment. Therefore, a full finite element model is established for the structural stress analysis. As shown in Fig. 4, the mesh discretisation of the model includes 10,809 20-node quadratic brick elements (Abaqus C3D20R) and 54,804 nodes with 3 elements in the thickness direction of the head crown and the nozzle.

To eliminate the influence of the boundary conditions on the mechanical behaviour of the nozzle junction, the lengths of the cylindrical shell and of the nozzle are approximately $1\times D_a$ and $3\times d_i$, respectively. The end of the cylindrical vessel is restrained in the vertical direction, but the nodes on this end can move in the radial direction. The fundamental mechanical loads include P_0, F_0, $M_{\text{in}0}$, $M_{\text{out}0}$, and T_0. The fundamental thermal load is determined by the temperature difference, $\Delta\theta_0$, where the temperatures of the outside and inside surfaces are 20 °C and 138 °C, respectively. The values of these fundamental loads are listed in Table 3. It should be noted that when considering the internal pressure, an additional equivalent axial tension is applied to the end of the nozzle. For convenience in applying the loads, the end surface of the nozzle is coupled to a master node using the Beam-type MPC constraint option within Abaqus. Thus, all of the nozzle loads are applied to this master node.

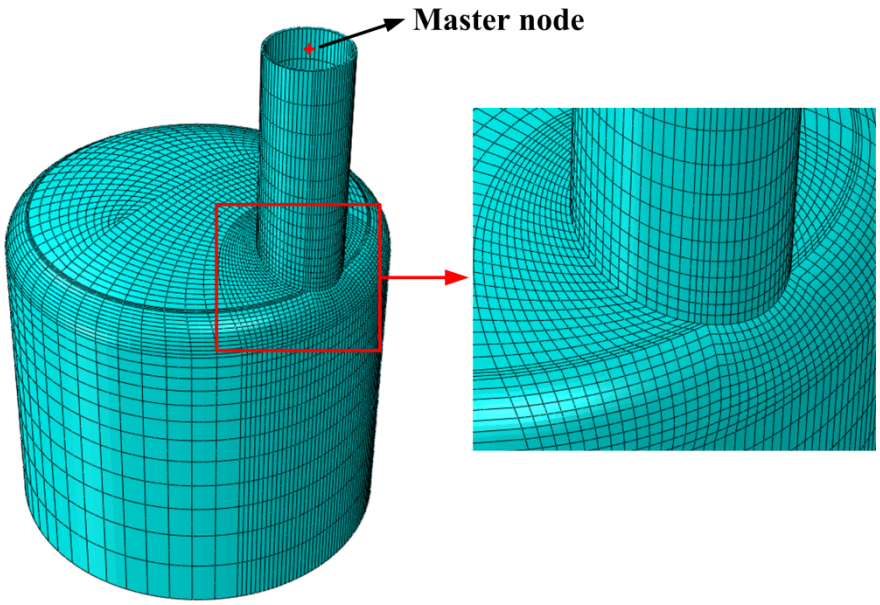

Fig. 4. Finite element model of the torispherical head with a piping nozzle with an enlarged view of the intersection between the torispherical head and nozzle.

Table 3 Fundamental loads applied to the torispherical head with a piping nozzle.

Internal pressure, P_0 [MPa]	5
Axial force, F_0 [kN]	2000
In plane bending moment, M_{in0} [kN·m]	400
Out-of-plane bending moment, M_{out0} [kN·m]	400
Twisting moment, T_0 [kN·m]	1000
Temperature difference, $\Delta\theta_0$ [°C]	118

3.2.2. Elastic stress calculation

To obtain the fictitious elastic stress field, $\boldsymbol{\sigma}^E(\boldsymbol{x})$, for the shakedown analysis, elastic analyses of the torispherical head with a piping nozzle under an internal pressure, axial force, twisting moment, out-of-plane and in-plane bending moments, and thermal loading are individually completed using Abaqus software. Calculation of the thermal elastic stress field is performed via an indirect coupling thermomechanical analysis as follows: 1) a heat transfer analysis is conducted to compute the temperature field of the structure; and 2) a structural stress analysis is performed to calculate the corresponding elastic stress field based on the obtained temperature distribution. The von Mises equivalent stress contours for the torispherical head with a piping nozzle under the six different individual loads are shown in Fig. 5.

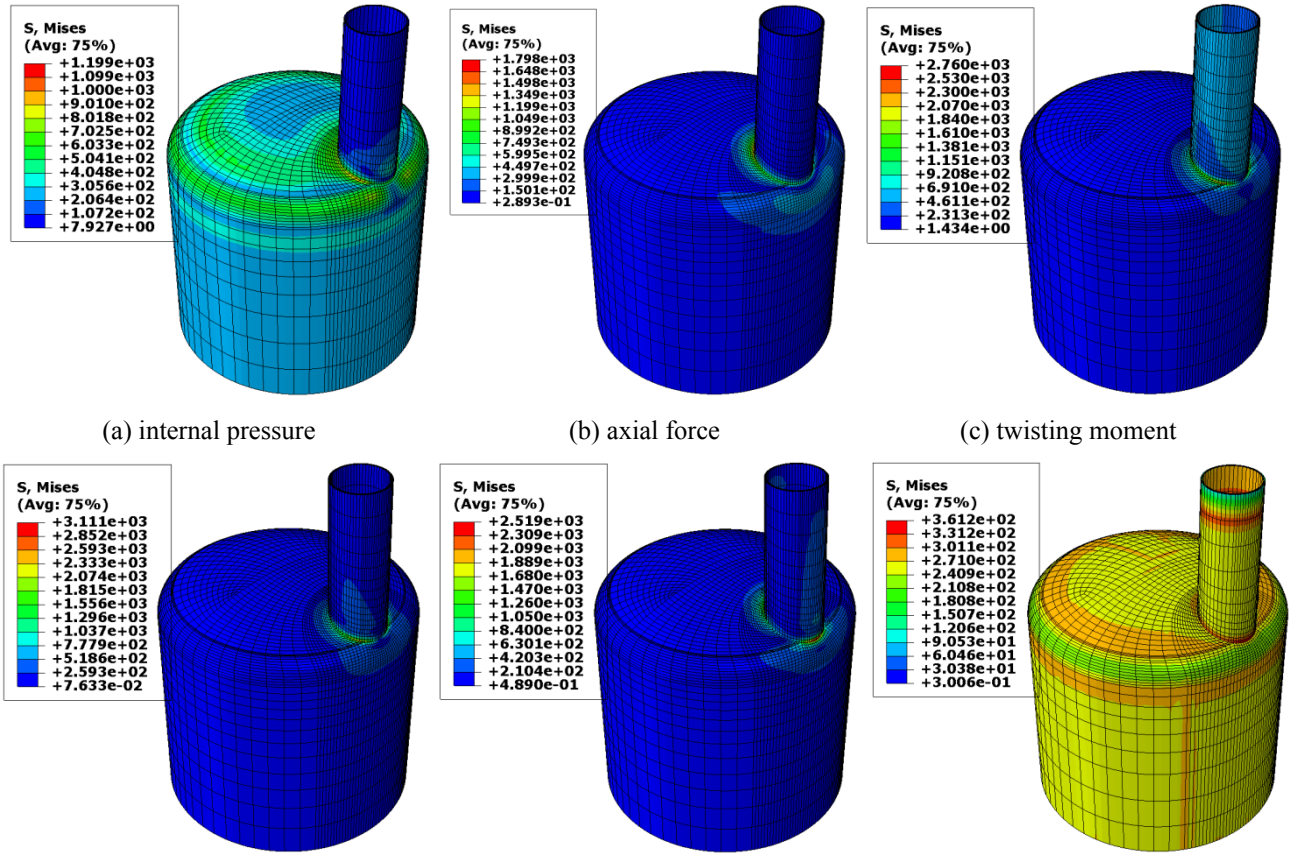

(a) internal pressure (b) axial force (c) twisting moment

(d) out-of-plane bending moment (e) in-plane bending moment (f) thermal loading

Fig. 5. Elastic stress contours of the torispherical head with a piping nozzle under six different individual loads.

3.3. Validation

The shakedown analysis algorithm can calculate the plastic limit load. When the number of load vertices is reduced to one, the calculated shakedown limit load is equal to the plastic limit load. SCM is used to calculate the plastic limit loads (one load vertex in Fig. 6a) and shakedown limit loads (two load vertices in Fig. 6b) of the torispherical head with a piping nozzle under six different individual loads, and the results are listed in Table 4. It is known that the shakedown limit load of a structure under a single load is the minimum of either its double elastic limit load or its plastic limit load. It should be noted that when the elastic-plastic incremental method in Abaqus is utilised to calculate the plastic limit loads, the 15-times elastic slope criterion [27] is adopted. The obtained results are compared in Table 4.

It can be observed from Table 4 that the shakedown limit loads calculated with the SCM are very close to the double elastic limit loads calculated with Abaqus and are less than the corresponding plastic limit loads. This indicates that the failure mechanisms of the torispherical head with a piping nozzle under the six different single cyclic loads are all alternating plasticity. The plastic limit loads calculated with the SCM also agree well with those calculated with the elastic-plastic incremental method. For the first five loading cases in Table 4, the

maximum relative error of the plastic limit loads calculated with the two methods is only 1.36%. It should be noted that thermal loading does not lead to plastic collapse of the structure.

Several researchers [14, 15, 27] have performed elastic stress, plastic limit and shakedown analyses of a torispherical head with a piping nozzle using different methods. For comparison, the available numerical results for this structure under different single loads are summarised in Table 5. It can be observed from Table 5 that the results of this study are approximately in agreement with the results reported by Hsieh et al. [27], Tran et al. [15], and Simon et al. [14], but the results of different results exhibit some discrepancies in the numerical values. These discrepancies result not only from the different methods used, but also from the different types of finite elements and sizes of element meshes selected. A simple way to illustrate these reasons is that different researchers have reported the different elastic limit loads listed in Table 5.

(a) loading path for the plastic limit load (b) loading path for the shakedown limit load

Fig. 6. Two loading paths under a single load.

Table 4 Shakedown limit and plastic limit loads calculated with two different methods.

Loading case	SCM		Abaqus	
	Shakedown limit load	Plastic limit load	Double elastic limit load	Plastic limit load
Pressure, P [MPa]	3.004	3.511	3.004	3.523
Axial force, F [kN]	833.8	1451.8	833.9	1463.2
Twisting moment, T [kN·m]	364.5	546.4	364.5	551.9
Out-of-plane moment, M_{out} [kN·m]	127.9	237.8	127.9	239.2
In-plane moment, M_{in} [kN·m]	107.6	248.7	107.7	252.1
Thermal loading, $\Delta\theta$ [°C]	236.0	---	236.0	---

Table 5 Comparison of the present results with results from literature.

Type	Loading case	Present	Hsieh [27]	Tran [15]	Simon [14]
Elastic limit load	Pressure [MPa]	1.502	1.370	1.600	1.524
	Axial force [kN]	416.9	450.0	399.0	483.1
	In-plane moment [kN·m]	53.9	64.7	64.6	55.4
	Out-of-plane moment [kN·m]	64.0	66.5	69.1	---

Shakedown limit load	Twisting moment [kN·m]	182.3	193.8	195.3	---
	Pressure [MPa]	3.004	---	3.200	3.047
	Axial force [kN]	833.8	---	798.0	965.9
	In-plane moment [kN·m]	107.6	---	129.2	110.7
	Out-of-plane moment [kN·m]	127.9	---	138.2	---
	Twisting moment [kN·m]	364.5	---	390.6	---
Plastic limit load	Pressure [MPa]	3.511	3.54	3.93	---
	Axial force [kN]	1451.8	1630.0	1492.0	---
	In-plane moment [kN·m]	248.7	282.6	256.0	---
	Out-of-plane moment [kN·m]	237.8	265.8	247.2	---
	Twisting moment [kN·m]	546.4	625.0	614.2	---

Table 6 Two-dimensional loading domains of interest for five loading combinations.

Loading combination	Loading domain
Pressure (P) and axial force (F)	(i) $0 \le F \le \mu_1^+ F_0$ and $0 \le P \le \mu_2^+ P_0$ (ii) $\mu_1^- F_0 \le F \le 0$ and $0 \le P \le \mu_2^+ P_0$
Pressure (P) and in-plane moment (M_{in})	(i) $0 \le M_{\text{in}} \le \mu_1^+ M_{\text{in0}}$ and $0 \le P \le \mu_2^+ P_0$ (ii) $\mu_1^- M_{\text{in0}} \le M_{\text{in}} \le 0$ and $0 \le P \le \mu_2^+ P_0$
Pressure (P) and out-of-plane moment (M_{out})	(i) $0 \le M_{\text{out}} \le \mu_1^+ M_{\text{out0}}$ and $0 \le P \le \mu_2^+ P_0$ (ii) $\mu_1^- M_{\text{out0}} \le M_{\text{out}} \le 0$ and $0 \le P \le \mu_2^+ P_0$
Pressure (P) and twisting moment (T)	(i) $0 \le T \le \mu_1^+ T_0$ and $0 \le P \le \mu_2^+ P_0$ (ii) $\mu_1^- T_0 \le T \le 0$ and $0 \le P \le \mu_2^+ P_0$
Pressure (P) and thermal loading ($\Delta\theta$)	(i) $0 \le \Delta\theta \le \mu_1^+ \Delta\theta_0$ and $0 \le P \le \mu_2^+ P_0$

4. Results and discussion

4.1. Shakedown domains under two-dimensional loading domains

The internal pressure, P, is the main load acting on the torispherical head with a piping nozzle. Here, the shakedown domains of the structure are investigated for combinations of the internal pressure with the five other loads, i.e. the internal pressure, P, with the axial force, F; internal pressure, P, with the in-plane bending moment, M_{in}; internal pressure, P, with the out-of-plane bending moment, M_{out}; internal pressure, P, with the twisting moment, T; and internal pressure, P, with the thermal loading, $\Delta\theta$. The two loads in each

of these combinations vary independently of each other within a quadrilateral loading domain (see Fig. 7). The five loading combinations and the corresponding loading domains of interest are listed in Table 6.

SCM is utilised to calculate the shakedown domains of the torispherical head with a piping nozzle under these five loading domains. The resulting two-dimensional shakedown domains are shown in Fig. 8Fig**. 12**. For comparison, the available numerical results from literature [14, 15, 27] are also plotted in these figures. It is observed from Fig. 8-Fig**. 12** that for the five loading combinations, the shapes of the shakedown boundary curves reported by different authors are all similar. The shakedown boundary curves obtained in this study are smooth, and the data points are evenly distributed in the line segment. This indicates that the numerical shakedown analysis results obtained with SCM are of high accuracy.

The shakedown boundary curves are all dominated by alternating plasticity, and the inflection points in the curves indicate that the failure appears in different locations on the structure. The points of intersection between the shakedown boundary curves and the coordinate axes represent the shakedown limit loads of the torispherical head with a piping nozzle under the corresponding single cyclic load, and these shakedown limit loads are the same as those given in Table 5.

As stated in Introduction, other numerical methods can be used to solve the shakedown problem. To clarify the differences in terms of the accuracy and computational cost of these methods, an LMM shakedown analysis is carried out. Taking a typical loading combination as an example, the shakedown domain of the torispherical head with a piping nozzle under the combination of an internal pressure and axial force is investigated. The two-dimensional shakedown domain calculated with LMM is shown in Fig. 8. It can be observed that the shakedown boundary curve obtained with LMM is very close to that obtained with SCM. These results illustrate that both methods have good accuracy. For the same loading case and finite element model, the CPU time needed to calculate the shakedown limit with LMM is approximately three times that required for SCM.

To verify that the failure behaviour of the structure is alternating plasticity when the magnitude of the applied load exceeds the computed shakedown limit, a step-by-step elastic-plastic incremental analysis is carried out. Two loading points (points “A” and “B” in Fig. 8) are selected as reference points. The effective plastic strains of a material point on the torispherical head with a piping nozzle over the first 30 load cycles for loading points “A” and “B” are shown in Fig. 13. For loading point “A”, a stable alternating plasticity behaviour is observed, while there is no further change in the effective plastic strain after the initial load cycles for loading point “B”.

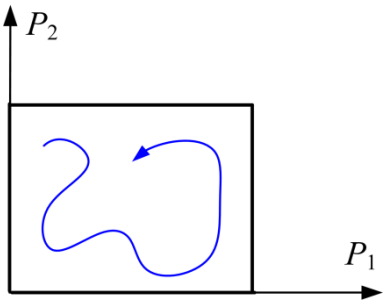

Fig. 7. Two loads vary independently of each other within a quadrilateral loading domain.

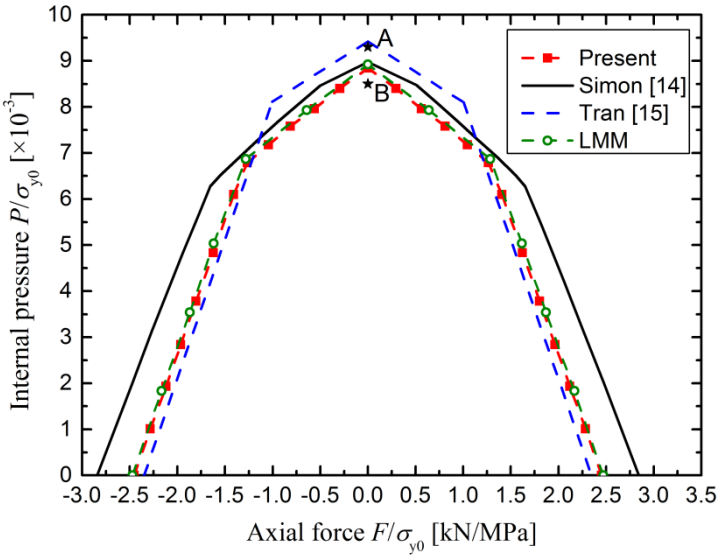

Fig. 8. Two-dimensional shakedown domains: internal pressure versus axial force.

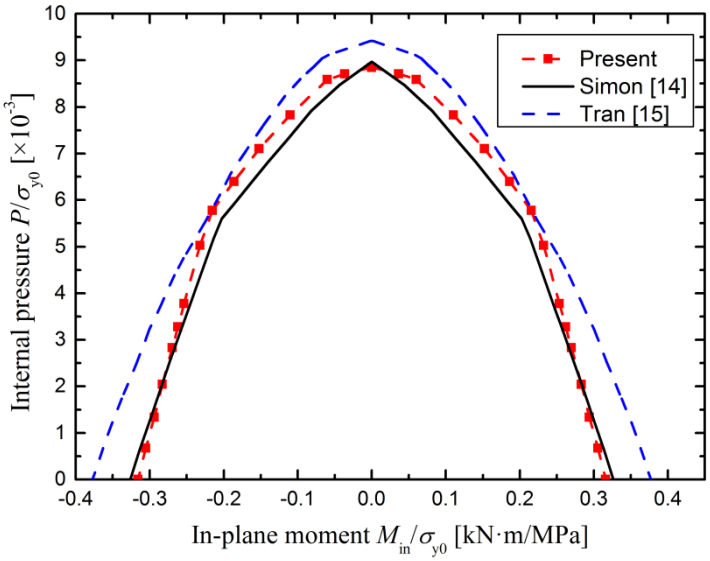

Fig. 9. Two-dimensional shakedown domains: internal pressure versus in-plane bending moment.

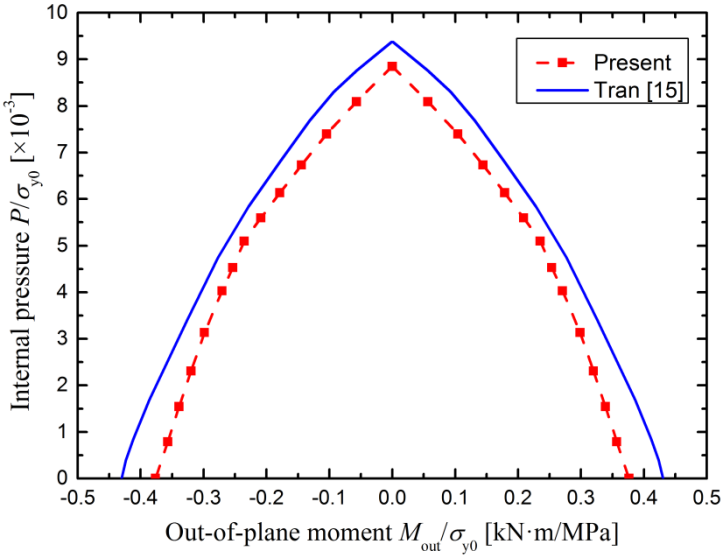

Fig. 10. Two-dimensional shakedown domains: internal pressure versus out-of-plane bending moment.

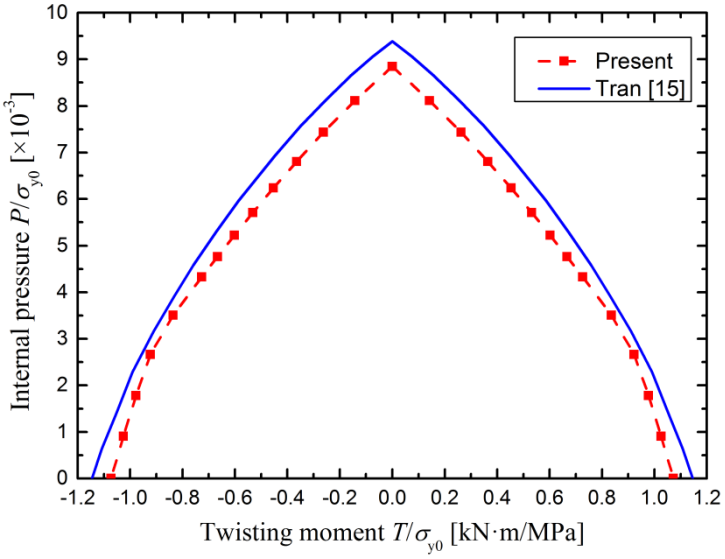

Fig. 11. Two-dimensional shakedown domains: internal pressure versus twisting moment.

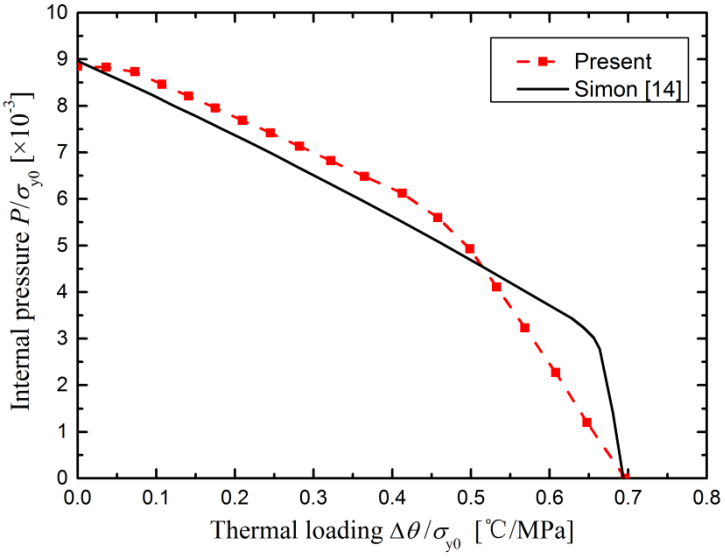

Fig. 12. Two-dimensional shakedown domains: internal pressure versus thermal loading.

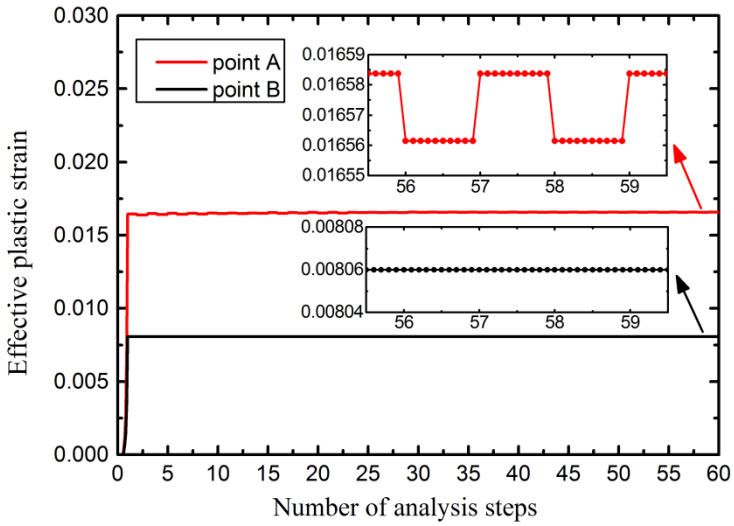

297

298 **Fig. 13.** Effective plastic strains of a point on the torispherical head with a piping nozzle over the first 30 load

299 cycles for loading points "A" and "B" plotted in Fig. 8.

300 **4.2. Shakedown domains under three-dimensional loading domains**

301 The shakedown domains of the torispherical head with a piping nozzle were also investigated under three-

302 dimensional loading domains. Each loading combination includes three loads, which are applied at the same

303 time and vary from zero to a maximum value independently of each other. The loading domain is same as that

304 shown in Fig. 1. Four loading combinations and the corresponding loading domains of interest are listed in

305 Table 7.

306 **Table 7** Three-dimensional loading domains of interest for the four different loading combinations

Loading combination	Loading domain
Pressure (P), axial force (F), and in-plane moment (M_{in})	$0 \le P \le \mu_1^+ P_0$, $0 \le F \le \mu_2^+ F_0$ and $0 \le M_{\text{in}} \le \mu_3^+ M_{\text{in}0}$
Pressure (P), axial force (F), and out-of-plane moment (M_{out})	$0 \le P \le \mu_1^+ P_0$, $0 \le F \le \mu_2^+ F_0$ and $0 \le M_{\text{out}} \le \mu_3^+ M_{\text{out}0}$
Pressure (P), axial force (F), and twisting moment (T)	$0 \le P \le \mu_1^+ P_0$, $0 \le F \le \mu_2^+ F_0$ and $0 \le T \le \mu_3^+ T_0$
Pressure (P), axial force (F), and thermal loading ($\Delta\theta$)	$0 \le P \le \mu_1^+ P_0$, $0 \le F \le \mu_2^+ F_0$ and $0 \le \Delta\theta \le \mu_3^+ \Delta\theta_0$

307

308 SCM is utilised to calculate the shakedown limit loads of the torispherical head with a piping nozzle under

309 different loading combinations. The three-dimensional shakedown domains corresponding to the four loading

310 domains of interest are shown in Fig. 14-Fig**. 17**. To sketch the shakedown boundary surface, more than 100

points representing the load vertex B^8 in Fig. 1 are selected. It should be noted that dimensionless coordinate values normalised to the yield strength are adopted to depict the shakedown boundary surface. In these figures, the red lines represent the intersections between the shakedown boundary surface and the coordinate planes. These red lines actually denote the shakedown boundary curves for the torispherical head with a piping nozzle under the specific two-dimensional loading domains. The residual stress field is also calculated when using SCM to perform the shakedown analysis. A typical von Mises equivalent residual stress field for the torispherical head with a piping nozzle is shown in Fig. 18.

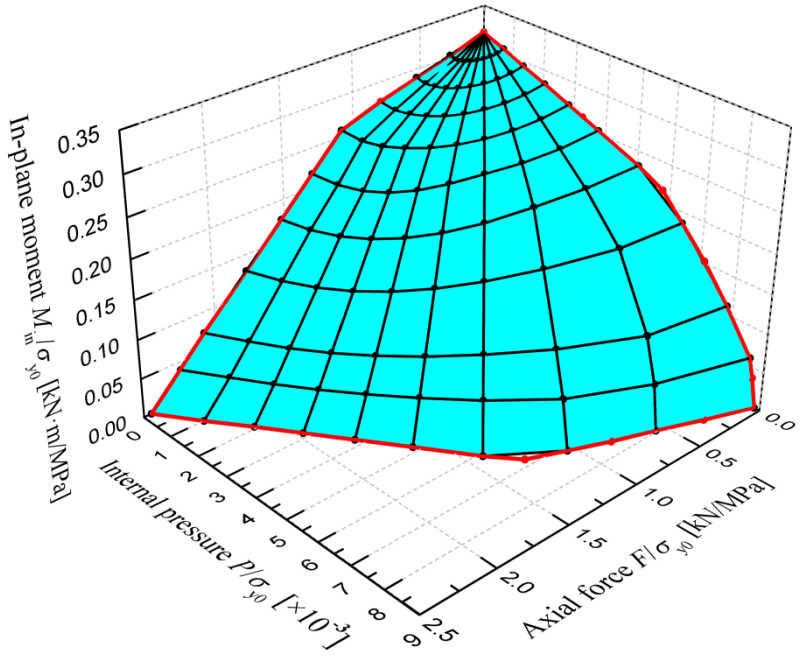

Fig. 14. Three-dimensional shakedown domain: in-plane bending moment, internal pressure, and axial force.

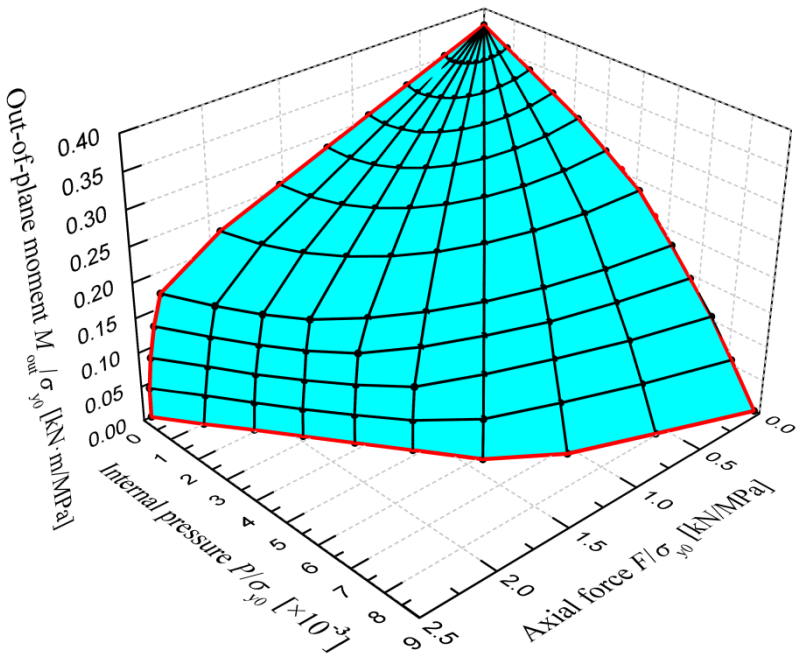

Fig. 15. Three-dimensional shakedown domain: out-of-plane bending moment, internal pressure, and axial force.

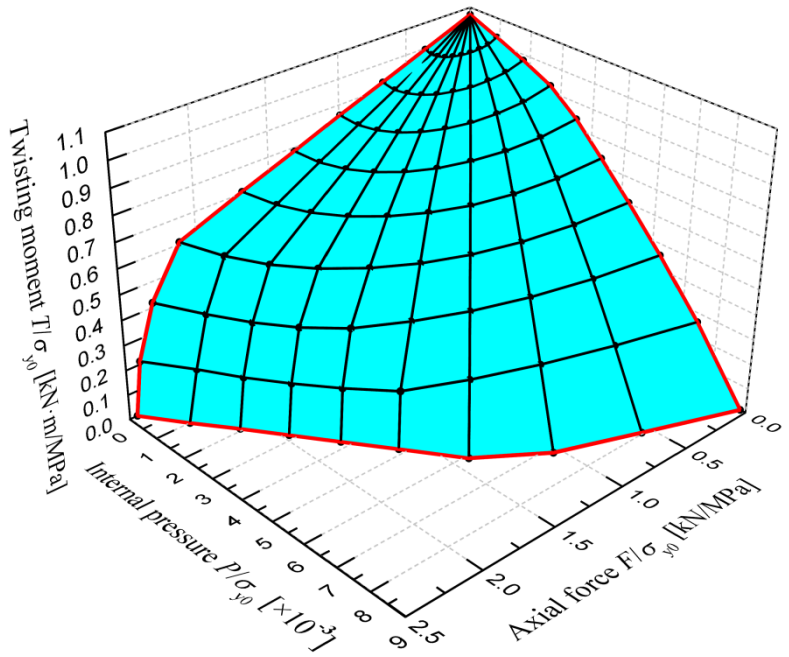

322

323 **Fig. 16.** Three-dimensional shakedown domain: twisting moment, internal pressure, and axial force.

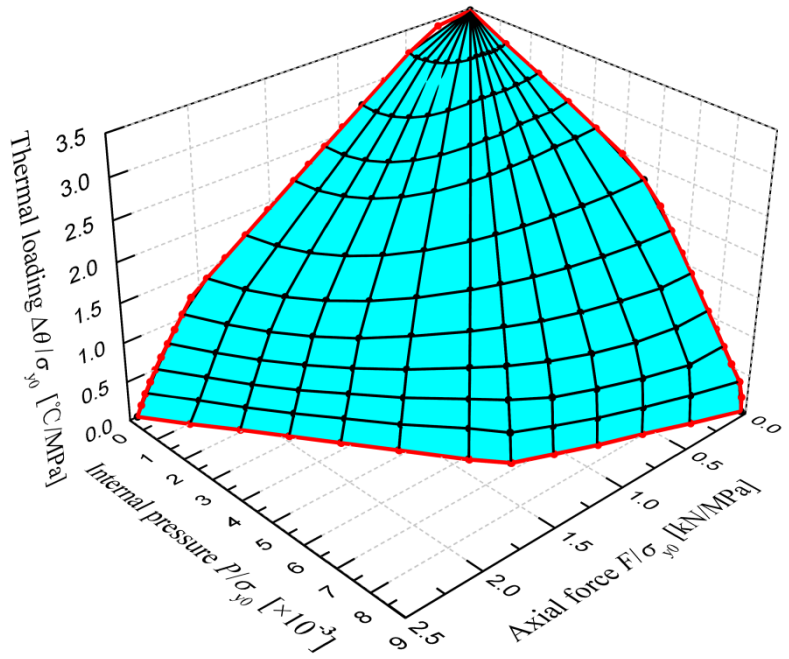

324

325 **Fig. 17.** Three-dimensional shakedown domain: thermal loading, internal pressure, and axial force.

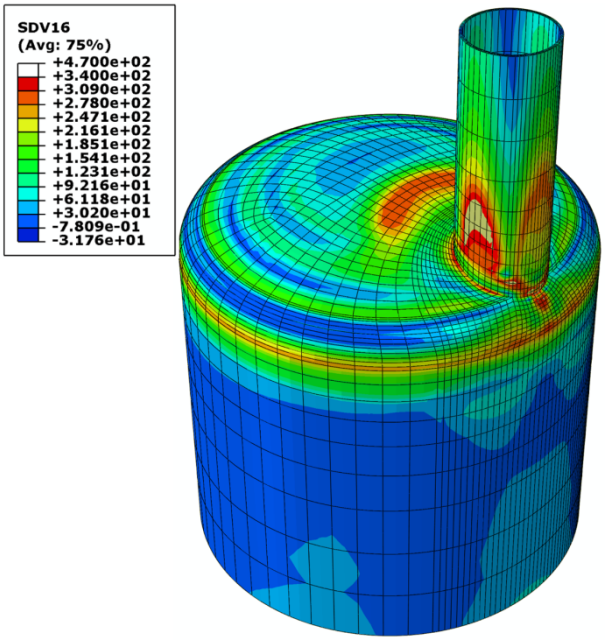

Fig. 18. Typical von Mises equivalent residual stress field for the torispherical head with a piping nozzle.

4.3. Shakedown domains considering the temperature-dependent yield strength

In the above examples, the material properties of the torispherical head with a piping nozzle are constant with respect to temperature (Table 2). To investigate the effect of a temperature-dependent yield strength on the shakedown domain, the yield strength, $\sigma_y(\theta)$, is considered as a linear function of the temperature, θ, as follows:

$$\sigma_y(\theta) = \sigma_{y_0} - 0.3 \times (\theta - 20\,^{\circ}\mathrm{C}) \tag{18}$$

For simplicity, only one loading case is considered. As expressed in Eq. (19), an internal pressure, P, axial force, F, and thermal loading, $\Delta\theta$, are applied at the same time, and vary from zero to a maximum value independently of each other.

$$0 \le P \le \mu_1^+ P_0,\ 0 \le F \le \mu_2^+ F_0 \text{ and } 0 \le \Delta\theta \le \mu_3^+ \Delta\theta_0 \tag{19}$$

In the shakedown analysis procedure, the temperature-dependent yield strength, $\sigma_y(\theta)$, is implemented at each Gauss integration point for all load vertices of a loading domain. The temperature field is updated at every iteration during calculation of the shakedown load multiplier. Both the mechanical and thermal loads are scaled. The resulting three-dimensional shakedown domain of the torispherical head with a piping nozzle considering the temperature-dependent yield strength, $\sigma_y(\theta)$, is shown as the green surface in Fig. 19. For comparison, the corresponding three-dimensional shakedown domain with a constant yield strength, σ_{y0}, is also shown in Fig. 19 (the cyan surface).

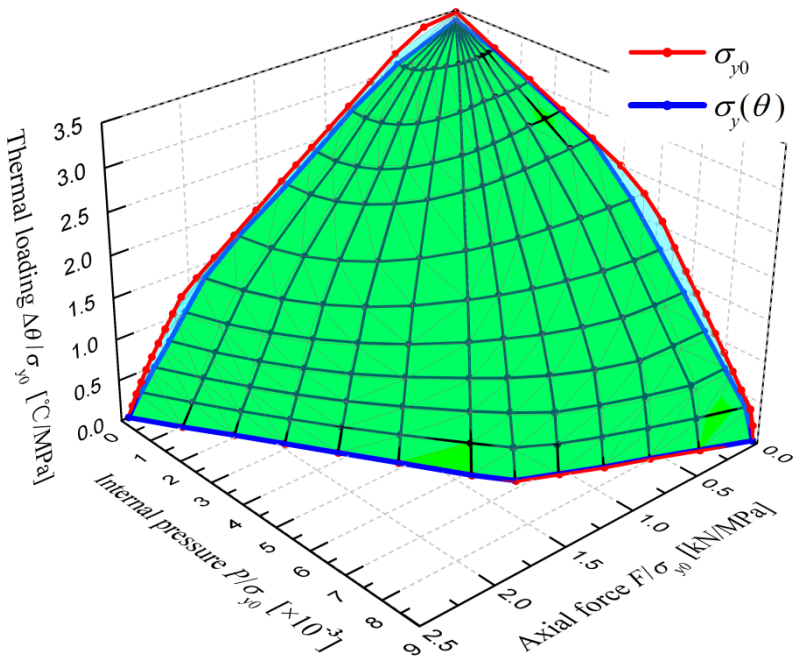

Fig. 19. Three-dimensional shakedown domain with a temperature-dependent yield strength: thermal loading, internal pressure, and axial force.

4.4. Discussion

To obtain the shakedown domains of the torispherical head with a piping nozzle under different loading combinations, approximately 700 shakedown analyses were performed using the SCM. For all of these shakedown analyses, the iterative SCM yielded good convergence. All of the calculations in this study were carried out in an Intel i7 computer environment with 16 GB of RAM.

According to the numerical results in Table 4, the shakedown limit loads calculated using SCM and the Abaqus elastic-plastic incremental method are in good agreement for the same finite element model, which illustrates the validity and high accuracy of the SCM. From Fig. 8-Fig**. 12**, it can be observed qualitatively that the shapes of the shakedown boundary curves under two-dimensional loading domains obtained in this study are similar to those reported by Hsieh et al. [27], Tran et al. [15], and Simon et al. [14]. The differences between the numerical values are due to the different methods and finite element models employed. In addition, two loading points located at different sides of the shakedown boundary curve are selected to validate the failure behaviour of the structure using Abaqus step-by-step cyclic loading simulations. For the loading cases considered in this study, the shakedown boundary curves are dominated by alternating plasticity.

It can be observed from Fig. 14-Fig**. 17** that the three-dimensional shakedown boundary surfaces are smooth and convex, and the data points on these surfaces are evenly distributed. This indicates the stability and reliability of the numerical results. The three-dimensional shakedown boundary surface contains some

information: 1) the points of intersection between the shakedown boundary surface and the coordinate axes can be used to determine the allowable range of a single load; 2) if the range of a specific load is known, the allowable ranges of the other two loads can be determined; 3) if the ranges of two specific loads are known, the allowable range of the third load can be determined. This information is of significance for safe engineering design.

It is evident from Fig. 19 that the shakedown domain is decreased when the temperature-dependent yield strength, $\sigma_y(\theta)$, is considered. However, there is some discrepancy in the amplitudes of this reduction in the shakedown limit loads for different loading cases. An explanation for these discrepancies is that the maximum stress point is not consistent with the maximum temperature point. Specifically, when the failure point is located on the outside surface of the torispherical head with a piping nozzle, at which the temperature remains constant at 20 °C, the shakedown limit load with consideration of the temperature-dependent yield strength is the same as that with a constant yield strength. When the failure point is located on the inside surface of the torispherical head with a piping nozzle, where the temperature changes with time, the shakedown limit load with consideration of the temperature-dependent yield strength is smaller than that with a constant yield strength.

Differing from the shakedown analysis methods using optimisation solvers, in which the running times are largely dependent on the loading scenario [9, 14], SCM is an iterative procedure based on a general finite element code, and the computing time has little relationship to the number of independent loads. To the best of the authors' knowledge, evaluation of the shakedown domain of a structure of comparable scale under a three-dimensional loading domain has only previously been reported in [14]. For a finite element model consisting of 6376 linear elements and 9645 nodes, the running time reported in [14] is less than 10 h. However, for the finite element model consisting of 10,809 quadratic elements and 54,804 nodes in this study, the CPU time for the SCM varies from 0.2 h to 0.4 h. Therefore, it can be said that SCM has huge computational advantages and is capable of solving the shakedown problem for large-scale practical engineering structures in a reasonable amount of time.

5. Conclusions

In this study, shakedown analyses of a torispherical head with a piping nozzle under the influence of an internal pressure, axial force, twisting moment, out-of-plane and in-plane bending moments, and thermal loading were carried out using the recently proposed SCM. Different loading combinations and a temperature-dependent yield strength are considered. Some conclusions are summarised as follows.

1. The numerical SCM is successfully implemented into the Abaqus platform and used to determine the shakedown domain of a torispherical head with a piping nozzle. The numerical results for the structure under a single load are validated with the elastic-plastic incremental method using Abaqus. The shakedown domains of the structure under two-dimensional loading domains calculated using SCM are compared with results from literature. The good agreement of the results with those in literature demonstrates the validity and high accuracy of the SCM.
2. The shakedown boundary surfaces of the torispherical head with a piping nozzle are analysed under four three-dimensional loading domains. These shakedown boundary surfaces can provide valuable guidance for the design and safety assessment of this structure.
3. The shakedown analysis of the torispherical head with a piping nozzle is investigated with consideration of a temperature-dependent yield strength. The observed reduction in the shakedown domain due to the effect of temperature on the yield strength is related to the position of the maximum stress point and the maximum temperature point.
4. The SCM overcomes problems involving dimensional obstacles that exist in most lower bound shakedown analysis methods. Its running time has little relationship with the dimension of the loading domains. All the numerical calculations yield a good convergence of the iterative process and demonstrate the applicability of the procedure. SCM is a powerful tool possessing huge computational advantages and is suitable for the shakedown analysis of large-scale structural components under complex multi-loading systems.

Acknowledgements

The authors gratefully acknowledge the support of the National Science Foundation for Distinguished Young Scholars of China (Grant No. 11325211) and the National Natural Science Foundation of China (Grant No. 11672147).

References

[1] Melan E. Zur Plastizität des räumlichen Kontinuums. Ingenieur-Archiv. 1938;9:116-26.
[2] Koiter WT. General theorems for elastic-plastic solids. In: Sneddon, JN, Hill, R, editors. Progress in Solid Mechanics: North-Holland: Amsterdam; 1960. p. 167-221.
[3] König JA. Shakedown of elastic-plastic structures. Warszawa, Poland: Elsevier; 1987.
[4] Weichert D, Ponter A. A historical view on shakedown theory. In: Stein E, editor. The History of Theoretical, Material and Computational Mechanics-Mathematics Meets Mechanics and Engineering: Springer; 2014. p. 169-93.
[5] Bisbos CD, Makrodimopoulos A, Pardalos PM. Second-order cone programming approaches to static shakedown

analysis in steel plasticity. Optim Method Softw. 2005;20:25-52.
[6] Liu YH, Zhang XF, Cen ZZ. Lower bound shakedown analysis by the symmetric Galerkin boundary element method. Int J Plasticity. 2005;21:21-42.
[7] Garcea G, Leonetti L. A unified mathematical programming formulation of strain driven and interior point algorithms for shakedown and limit analysis. Int J Numer Meth Eng. 2011;88:1085-111.
[8] Simon JW, Weichert D. Numerical lower bound shakedown analysis of engineering structures. Comput Method Appl M. 2011;200:2828-39.
[9] Simon JW, Weichert D. Shakedown analysis with multidimensional loading spaces. Comput Mech. 2012;49:477-85.
[10] Zhang Y. An iteration algorithm for kinematic shakedown analysis. Comput Method Appl M. 1995;127:217-26.
[11] Casciaro R, Garcea G. An iterative method for shakedown analysis. Comput Method Appl M. 2002;191:5761-92.
[12] Zouain N, Borges L, Silveira JL. An algorithm for shakedown analysis with nonlinear yield functions. Comput Method Appl M. 2002;191:2463-81.
[13] Vu DK, Yan AM, Nguyen-Dang H. A primal–dual algorithm for shakedown analysis of structures. Comput Method Appl M. 2004;193:4663-74.
[14] Simon JW, Chen G, Weichert D. Shakedown analysis of nozzles in the knuckle region of torispherical heads under multiple thermo-mechanical loadings. International Journal of Pressure Vessels and Piping. 2014;116:47-55.
[15] Tran TN, Kreißig R, Vu DK, Manfred S. Upper bound limit and shakedown analysis of shells using the exact Ilyushin yield surface. Comput Struct. 2008;86:1683-95.
[16] Seshadri R, Mangalaramanan SP. Lower bound limit loads using variational concepts: The m(alpha)-method. International Journal of Pressure Vessels and Piping. 1997;71:93-106.
[17] Mackenzie D, Boyle JT, Hamilton R. The elastic compensation method for limit and shakedown analysis: a review. J Strain Anal Eng. 2000;35:171-88.
[18] Ponter ARS, Carter KF. Shakedown state simulation techniques based on linear elastic solutions. Comput Method Appl M. 1997;140:259-79.
[19] Adibi-Asl R, Reinhardt W. Non-cyclic shakedown/ratcheting boundary determination - Part 1: Analytical approach. International Journal of Pressure Vessels and Piping. 2011;88:311-20.
[20] Adibi-Asl R, Reinhardt W. Non-cyclic shakedown/ratcheting boundary determination - Part 2: Numerical implementation. International Journal of Pressure Vessels and Piping. 2011;88:321-9.
[21] Abdalla HF. Shakedown boundary determination of a 90° back-to-back pipe bend subjected to steady internal pressures and cyclic in-plane bending moments. International Journal of Pressure Vessels and Piping. 2014;116:1-9.
[22] Spiliopoulos KV, Panagiotou KD. An enhanced numerical procedure for the shakedown analysis in multidimensional loading domains. Comput Struct. 2017;193:155-71.
[23] Chen HF, Ponter ARS. Shakedown and limit analyses for 3-D structures using the linear matching method. International Journal of Pressure Vessels and Piping. 2001;78:443-51.
[24] Chen HF, Ponter ARS. Integrity assessment of a 3D tubeplate using the linear matching method. Part 1. Shakedown, reverse plasticity and ratchetting. International Journal of Pressure Vessels and Piping. 2005;82:85-94.
[25] Peng H, Liu Y, Chen H. A numerical formulation and algorithm for limit and shakedown analysis of large-scale elastoplastic structures. Comput Mech. 2018. (in press) https://doi.org/10.1007/s00466-018-1581-x
[26] Saal H, Bauer H, Häderle M-U. Flexibility factors for nozzles in the knuckle region of dished pressure vessel heads. International Journal of Pressure Vessels and Piping. 1997;70:151-60.
[27] Hsieh MF, Moffat DG, Mistry J. Nozzles in the knuckle region of a torispherical head: limit load interaction under combined pressure and piping loads. International Journal of Pressure Vessels and Piping. 2000;77:807-15.
[28] Hsieh MF, Moreton DN, Mistry J, Moffat DG. Limit loads for knuckle-encroaching nozzles in torispherical heads: experimental verification of finite element predictions. J Strain Anal Eng. 2002;37:313-26.
[29] ABAQUS. Dassault Systems, version 6.14, 2014.
[30] Gokhfeld DA, Charniavsky OF. Limit analysis of structures at thermal cycling. Sijthoff & Noordhoff ed. The

Netherlands: Alphen aan den Rijn; 1980.